Autores: M. Aranda, Y. Mezouar, G. Lopez-Nicolas, C. Sagues
Título: Scale-Free Vision-Based Aerial Control of a Ground Formation with Hybrid Topology
IEEE Transactions on Control System Technology (ISSN 1063-6536), doi: 10.1109/TCST.2018.2834308.
Vol. 27(4): 1703-1711, 2019

Scale-Free Vision-Based Aerial Control of a Ground Formation With Hybrid Topology

Miguel Aranda, Youcef Mezouar, Gonzalo López-Nicolás, and Carlos Sagüés

***Abstract*— We present a novel vision-based control method to make a group of ground mobile robots achieve a specified formation shape with unspecified size. Our approach uses multiple aerial control units equipped with downward-facing cameras, each observing a partial subset of the multirobot team. The units compute the control commands from the ground robots' image projections, using neither calibration nor scene scale information, and transmit them to the robots. The control strategy relies on the calculation of image similarity transformations, and we show it to be asymptotically stable if the overlaps between the subsets of controlled robots satisfy certain conditions. The presence of the supervisory units, which coordinate their motions to guarantee a correct control performance, gives rise to a hybrid system topology. All in all, the proposed system provides relevant practical advantages in simplicity and flexibility. Within the problem of controlling a team shape, our contribution lies in addressing several simultaneous challenges: the controller needs only partial information of the robotic group, does not use distance measurements or global reference frames, is designed for unicycle agents, and can accommodate topology changes. We present illustrative simulation results.**

***Index Terms*— Distributed algorithms, mobile robots, multirobot systems, robot vision systems, unmanned aerial vehicles.**

I. Introduction

COMPARED with single-robot setups, multirobot systems provide increased efficiency and reliability, which makes them a very popular research subject. We address here the particular problem of formation shape control, where multiple robots move to collectively form a desired shape with unspecified location, rotation, and size [1]. As opposed to team formations defined as rigid, fixed-size patterns of agent positions [2]–[6], we study here formations specified only by angular constraints, also known in the literature as *bearing formations*. Controlling them is a problem of current interest [7]–[15], crucial in any application scenario where only angular measurements are available. Also, such a shape control allows, e.g., to regroup the agents in an organized manner before addressing a subsequent task, to create desired vicinities (with no specific regard for distances) between concrete agents, or to form a certain favorable shape as fast as possible, e.g., in reaction to a threat. Here, we investigate this relevant problem considering an infrastructure-free scenario, in the sense that the proposed robotic system does not depend on any elements external to itself (e.g., GPS or motion capture data), which is interesting in practice for flexibility and robustness. To this end, the use of vision sensors is quite appealing. Cameras naturally lend themselves to angle-based control and enable various multirobot behaviors, e.g., coordinated motion [16] and orientation alignment [17]. Aerial vision has been identified as particularly interesting for control and environment perception tasks in robotics [18]–[25] due to cameras being low-weight sensors that provide very rich data.

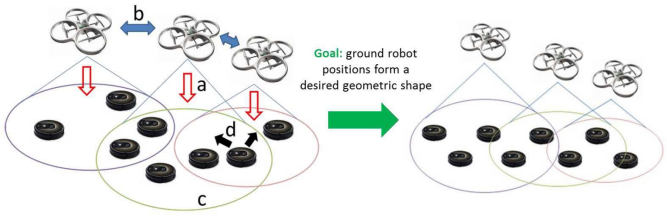

Fig. 1. Overview of the multirobot control system. Multiple (three, in this example) moving aerial units are used. Each computes (Section III) and transmits (a) motion commands for a set of ground robots in its camera's field of view (c). The robots that are controlled by multiple cameras combine the multiple received commands (d) to obtain their motion input, as described in Section IV. The UAVs can communicate (b) to coordinate their actions. The control task is for the ground robots' positions to form a specified shape.

A. Properties of the Aerial Vision-Based Framework

We build here on a control framework of ground formations with a specified size that we presented in [21] and [23]. Our method is based on a two-layer architecture where a set of downward-facing cameras onboard unmanned aerial vehicles (UAVs) are used to observe and control the ground robots. The system setup proposed is illustrated in Fig. 1. The aerial units detect and identify the robots and measure their position and heading, using image information. They compute a similarity from their current image and a template image (which encodes the desired shape) to define the motion goals for the ground robots. Crucially, each UAV controls only a partial *subset* of the robots and uses solely uncalibrated image information. No common reference frame among UAVs is needed, and they can displace and rotate while hovering throughout execution without affecting the control convergence.

Manuscript received August 4, 2017; revised January 31, 2018; accepted April 12, 2018. Manuscript received in final form May 3, 2018. This work was supported in part by the French Government via programs FUI (Project Aerostrip) and Investissements d'Avenir (I-SITE Project CAP 20-25—MaRoC), and in part by the Spanish Government/European Union through Project DPI2015-69376-R. Recommended by Associate Editor A. Tayebi. *(Corresponding author: Miguel Aranda.)*

M. Aranda and Y. Mezouar are with Université Clermont Auvergne, CNRS, SIGMA Clermont, Institut Pascal, F-63000 Clermont-Ferrand, France (e-mail: miguel.aranda@sigma-clermont.fr; youcef.mezouar@sigma-clermont.fr).

G. López-Nicolás and C. Sagüés are with the Instituto de Investigación en Ingeniería de Aragón, Universidad de Zaragoza, 50018 Zaragoza, Spain (e-mail: gonlopez@unizar.es; csagues@unizar.es).

Color versions of one or more of the figures in this paper are available online at http://ieeexplore.ieee.org.

Digital Object Identifier 10.1109/TCST.2018.2834308

These prominent practical advantages facilitate simple, robust, and flexible implementation (see Section VIII). We require certain overlaps between subsets and establish how a ground robot receiving multiple commands integrates them to compute its movement. Via Lyapunov-based analysis, we show that the proposed controller makes the team asymptotically reach the prescribed shape. We also provide a method for the UAVs to control their motions to appropriately cover the ground agents. In terms of *topology* (i.e., the interactions between elements of the multiagent system), our framework is *hybrid*; this means that it is neither centralized (there are multiple UAVs, each handling partial information) nor purely distributed, because each UAV acts as a central node for a subset of robots.

B. Related Literature on Formation Shape Control

The literature on the noncentralized control of bearing formations requires each agent to satisfy desired angular constraints with respect to a subset of the other agents. To guarantee the achievement of the prescribed team shape, the interaction graph that encapsulates the system's topology must satisfy *parallel (or bearing) rigidity* conditions. Within this framework, [8], [9], and [11] present distributed control laws for these formations relying only on angular measurements, while in [7], distances are also used. The work [13] uses only bearings and requires the robots to synchronize their orientations during execution. All these approaches need the relative angles used by the agents to be expressed in a common orientation reference, contrary to our method, where the measurements are expressed in the different and independent image frames of the multiple cameras. Importantly, in these related methods, the final team shape has a constrained orientation in the workspace. For numerous applications (e.g., team navigation in formation), a pattern with no constraints on its orientation—as allowed by our method—is more flexible and efficient. The controller in [14] stems from the principles of the SE(2) rigidity theory. Each agent uses locally expressed bearings and the relative orientation of neighboring agents' frames. The scheme in [12] employs a topological representation via the complex graph Laplacian and also controls the team shape without global references, albeit using both angles and distances. Similar information is assumed in [10] and [15], which deal with formations of adjustable size. The topology of the system may change over time, and the study of such changes is a prevalent topic [26], [27]. Unlike in the works cited above, here we investigate this *switching topology* scenario, and we assume that the ground robots have nonholonomic (unicycle) kinematics.

C. Statement of Contributions

Relative to the literature on formation shape control, our contribution lies in that we consider more challenging conditions. Specifically, our noncentralized, partial information-based method requires no global reference frames and relies solely on pixel image information and no range measurements. We consider unicycle agents and study the stability under switching topologies. Also, our proposed hybrid architecture represents a novel perspective on the problem, with practical advantages in, e.g., ground robot simplicity, task supervision, and flexibility, discussed in Section VIII.

Our previous method proposed in [23] also considers a two-layer framework and a similar scenario, controlling a fixed-size ground formation with cameras that can perform team scale adjustments using supplementary information. In this brief, we present the following novel contributions relative to that work.

1) Here, the size of the obtained formation is flexible, a property that cannot be achieved with the method in [23], and that is significant and interesting in its own right. It can, e.g., increase the motion efficiency and reduce the task execution time.
2) The approach has significantly lower information requirements. The aerial units use only pixel coordinates of the images of the ground robots, and no information of absolute scale. Camera calibration, metric data, or image scale estimates obtained with supplementary information are not needed. In contrast, [23] requires some of these sources of information to obtain continuous knowledge of the scale of the imaged scene.
3) In contrast with [23], here we provide formal stability guarantees under switching topologies, which is an important aspect as topology switches will typically occur in practice.

II. System Description and Operating Assumptions

Let us describe the characteristics of the proposed system and the conditions of operation that are assumed.

A. Task

The positions of a set, S, of n mobile robots must attain a prescribed shape, with unspecified size.

B. Architecture

The system has a two-layer architecture: the ground robot layer, and a set of m UAVs that observe the robots and control their motion.

C. Vehicle Dynamics

Each UAV remains near-hovering (i.e., its yaw axis is maintained vertical) and its translation is commanded via kinematic control (as in [28]; see details in Section VI). The ground robots have unicycle kinematics and move on a horizontal ground plane.

D. Perception

Each UAV carries a fixed perspective camera facing downward. Using vision processing, it can detect and identify those ground robots in its field of view and compute their image positions and headings. The ground robots do not require any sensors for the task addressed.

E. Prior Information

Each aerial unit knows the prescribed formation shape, with the identification of each robot, represented in the form of a *template image* (Section III).

F. Communications

Each UAV sends commands via wireless communication to robots in its camera's field of view. Two UAVs that observe robots in common at any time communicate via wireless to coordinate their motions/actions (see Section II-H), and multihop exchanges may also be used. The ground robots do not transmit any data.

G. Topology

The control topology is hybrid (not centralized, not purely distributed). For system stability purposes, we characterize it as follows. Each UAV views a subset of robots $S_j \subseteq S$, $j = 1, \ldots, m$ and controls a set $S_j^c \subseteq S_j$, being these sets time-varying. Formation achievement requires overlaps between these sets. We define $\mathcal{G}_c$ as an undirected graph where each node is a UAV and there is an edge (j, k) if $\text{card}(S_j^c \cap S_k^c) \geq 2$ (i.e., the two UAVs are controlling at least two common robots). We define the following *topological conditions*.

1) *TC1:* $\mathcal{G}_c$ is connected.
2) *TC2:* $\bigcup_{j=1,\ldots,m} S_j^c = S$ (i.e., every robot is controlled).
3) *TC3:* $\text{card}(S_j^c \bigcap S_k^c) = 2$ if j and k are neighbors in $\mathcal{G}_c$, 0 otherwise (i.e., neighboring UAVs share exactly two robots, and nonneighboring UAVs share no robots).
4) *TC4:* $S_j^c \bigcap S_k^c \bigcap S_l^c = \emptyset$ if j, k, and l are all different. That is, the intersections between the sets are mutually disjoint.
5) *TC5:* $\mathcal{G}_c$ is a tree.

We define $\mathcal{P}$ as the set of all possible topologies that satisfy TC1, TC2, TC3, TC4, and TC5, and $\mathcal{Q}$ as the set of those topologies that satisfy TC1 and TC2. We denote the system's topology at time t by $p(t)$. We assume $p(t = 0) \in \{\mathcal{P} \cup \mathcal{Q}\}$.

H. Coordination and Control

Ground Robots: They integrate and follow the motion commands received from the UAVs (Section IV). They do not sense/communicate with one another but move in coordination thanks to the aerial units. *Aerial Units:* Each unit j sends a motion objective, and image distance information—obtained as shown in Section IV—to each robot in S_j^c. Each UAV coordinates its motion and the definition of S_j and S_j^c with its neighbors (in terms of the graph $\mathcal{G}_c$) to maintain $p(t)$ within the set $\mathcal{P}$ (Section VI). They also ensure that each topology is active for a lower bounded time span.

III. Similarity-Based Motion Goals Computation

Consider next a given control unit j. To compute the control goals for the ground robots, it uses two perspective images.

1) The *template image* is a predefined, fixed top view, with arbitrary scale, of the desired formation shape. Each robot is represented by a point $\mathbf{p}_\mathbf{i}'$ in pixel coordinates. Unit j only uses those points in the template image that correspond to robots j controls (i.e., $i \in S_j^c$).
2) The *current image* is a top view of the current configuration of the subset of robots $i \in S_j^c$, each of which is represented by a point, $\mathbf{p}_\mathbf{i}^\mathbf{j}$, in pixels.

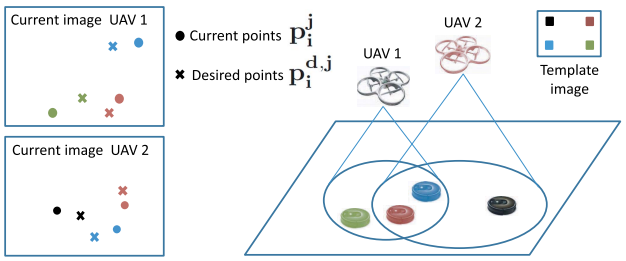

Fig. 2. Each UAV (i.e., 1 or 2) sees and controls only a partial subset of robots, using the corresponding partial set of template and current image points to compute the desired image points via a least-squares similarity.

Algorithm 1 Computation by Camera j at Each Time Instant of the Desired Image Positions for the Robots $i \in S_j^c$

1) Select the points $\mathbf{p}_\mathbf{i}'$ for $i \in S_j^c$ from the *template image* and (if required) translate them to make their centroid zero, obtaining the set of points $\mathbf{p}_\mathbf{ic}^{\prime\mathbf{j}}$.
2) **While** control executes **do**:
   a) Acquire a new *current image*.
   b) Detect and identify in the current image the points $\mathbf{p}_\mathbf{i}^\mathbf{j}$ corresponding with the current robot positions.
   c) Subtract the centroid, $\mathbf{c}_\mathbf{p}^\mathbf{j}$, of the points $\mathbf{p}_\mathbf{i}^\mathbf{j}$, to create a new set of points $\mathbf{p}_\mathbf{ic}^\mathbf{j}$ with zero centroid.
   d) Compute the similarity $\mathbf{H}_\mathbf{s}^\mathbf{j}$ that, applied on $\mathbf{p}_\mathbf{ic}^{\prime\mathbf{j}}$, aligns them with $\mathbf{p}_\mathbf{ic}^\mathbf{j}$ with least-squares error [29].
   e) Compute the desired image points, expressed in the current image, as: $\mathbf{p}_\mathbf{i}^{\mathbf{d,j}} = \mathbf{H}_\mathbf{s}^\mathbf{j}\, \mathbf{p}_\mathbf{ic}^{\prime\mathbf{j}} + \mathbf{c}_\mathbf{p}^\mathbf{j}$.

We propose a strategy where each camera uses the template and current image points to compute a *similarity* transformation (translation, rotation, and scaling) that aligns them with least-squares error [29]. The 2-D similarity we calculate relating the two point sets is parameterized as follows:

$$\mathbf{H}_\mathbf{s}^\mathbf{j} = \begin{bmatrix} s_j \cos\phi_j & -s_j \sin\phi_j \\ s_j \sin\phi_j & s_j \cos\phi_j \end{bmatrix} \tag{1}$$

and encodes the rotation of the template shape by $\phi_j \in [-\pi, \pi)$ and its scaling by $s_j \in \mathbb{R}^+$. This, together with a translation such that the current points' centroid is maintained, is used to obtain what we call the *desired* points, $\mathbf{p}_\mathbf{i}^{\mathbf{d,j}}$, which define the robots' motion goals. Algorithm 1 summarizes the process and Fig. 2 illustrates it for two different UAVs. A key decoupling between camera motion and ground control is expressed next.

Property 1: The ground positions associated with the desired points, defined from the optimal similarity by a given camera, are invariant to the downward-facing camera's position, orientation, and calibration.

Proof: Consider two arbitrary configurations for camera j: j_a and j_b. These can be linked by a similarity $\mathbf{G_{ba}}$, so $\mathbf{p}_\mathbf{ic}^{\mathbf{j_b}} = \mathbf{G_{ba}}\mathbf{p}_\mathbf{ic}^{\mathbf{j_a}}$ for $i \in S_j^c$. Obviously, $\mathbf{p}_\mathbf{ic}^{\prime\mathbf{j_b}} = \mathbf{p}_\mathbf{ic}^{\prime\mathbf{j_a}}$. The similarity (1) can be obtained for $k = a$ or b solving via least squares a linear system with equations: $\mathbf{H}_\mathbf{s}^{\mathbf{j_k}}\mathbf{p}_\mathbf{ic}^{\prime\mathbf{j_k}} - \mathbf{p}_\mathbf{ic}^{\mathbf{j_k}} = \mathbf{0}\ \forall i \in S_j^c$. Comparing the two systems, we have $\mathbf{H}_\mathbf{s}^{\mathbf{j_b}} = \mathbf{G_{ba}}\mathbf{H}_\mathbf{s}^{\mathbf{j_a}}$.

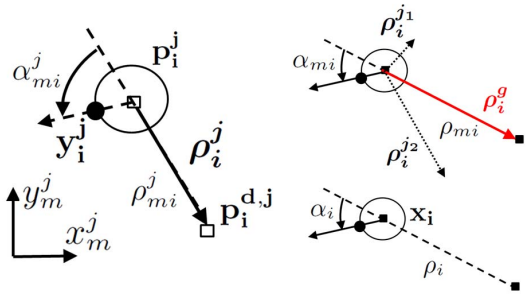

Fig. 3. Left: geometric variables and control vector computed for robot i by camera j, defined in its image. Top right: representation of $i's$ global motion vector computed from image information received from two cameras j_1 and j_2. Bottom right: state of the robot on the ground plane.

Then (see Algorithm 1), $\mathbf{p_i^{d,j_b}} - \mathbf{c_p^{j_b}} = \mathbf{H_s^{j_b}}\mathbf{p_{ic}^{'j_b}} = \mathbf{G_{ba}}\mathbf{H_s^{j_a}}\mathbf{p_{ic}^{'j_a}} = \mathbf{G_{ba}}(\mathbf{p_i^{d,j_a}} - \mathbf{c_p^{j_a}})$, where clearly $\mathbf{c_p^{j_a}}$ and $\mathbf{c_p^{j_b}}$ are the centroids of the desired point sets. Hence, the desired points i for a and b are projections of the same ground position $\forall i \in S_j^c$. ■

If $\mathbf{p_i^j} = \mathbf{p_i^{d,j}}$ $\forall i \in S_j^c$, clearly, the robots in this *subset* form the desired *subshape*. Our control goal is thus to move them so that they meet this condition. Note, however, the important challenges we face: these subshapes must fit together in the *full* formation (*overlaps* between subsets are needed), and a robot can receive *multiple partial and inconsistent* motion goals—see, e.g., the two robots in the intersection in Fig. 2. Section IV describes how these issues are solved.

IV. Coordinated Ground Robot Control Scheme

We explain next how a control unit j computes the information to be sent to a controlled robot i. Given a camera with usual characteristics, we can define a scale $r_j > 0$ (in pixels/m units) relating j's image distances with the metric distances between ground entities. This scale is unknown, freely time-varying, and different for each camera.

The parameters of the control scheme are depicted in Fig. 3. Using the strategy described in Section III, we can define $\mathbf{p_i^{d,j}}$ in the current image and compute the vector

$$\boldsymbol{\rho}_i^j = \mathbf{p_i^{d,j}} - \mathbf{p_i^j}. \tag{2}$$

By detecting the robots' positions and orientations in the images captured by its onboard camera, the control unit can obtain $\rho^j_{\text{mi}} = \|\mathbf{p_i^{d,j}} - \mathbf{p_i^j}\|$, and it can also define the unit vector $\widehat{\boldsymbol{\rho}}_i^j = \boldsymbol{\rho}_i^j / \rho^j_{\text{mi}}$ and the unit vector in the direction of the robot's heading (which j measures in the image) $\mathbf{y_i^j}$. Then, the control unit can compute the following angular parameter:

$$\alpha^j_{\text{mi}} = \text{atan2}\left(-\left[\begin{pmatrix}\widehat{\boldsymbol{\rho}}_i^j \\ 0\end{pmatrix} \times \begin{pmatrix}\mathbf{y_i^j} \\ 0\end{pmatrix}\right]_z, -\widehat{\boldsymbol{\rho}}_i^{j^T}\mathbf{y_i^j}\right) \tag{3}$$

where $[\cdot]_z$ denotes the z-axis coordinate. From ρ^j_{mi} and α^j_{mi}, unit j obtains $\boldsymbol{\rho}_i^j$ expressed in i's frame and sends it to i.

A. Combination of Multicamera Commands

Robot i may receive from multiple cameras simultaneous control goals that are inconsistent: each vector $\boldsymbol{\rho}_i^j$ for different j values is computed from a different subset of robots—so it will point in a different direction—and is also associated with a different scale r_j.

To solve the scale inconsistency, unit j sends robot i the identification of the robots that are closest to it in j's image (i.e., its physical nearest neighbors, in any direction around the robot), and the value of the image distances between i and each of these robots (i.e., $\|\mathbf{p_i^j} - \mathbf{p_{i_o}^j}\|$ for a given neighbor i_o). From TC3, robot i can compute the scale ratio between all cameras it receives data from: assume that aerial unit k also sends data to robot i and that a robot i_o is a physical neighbor of i; both j and k view i and i_o. Then, i can compute the relative scale as follows: $r_{kj} = r_k / r_j = \|\mathbf{p_i^k} - \mathbf{p_{i_o}^k}\| / \|\mathbf{p_i^j} - \mathbf{p_{i_o}^j}\|$.

We define the global motion vector that robot i computes as a weighted sum that integrates all its motion goals

$$\boldsymbol{\rho}_i^g = \frac{1}{\text{card}(C_i)} \sum_{j \in C_i} \left[\sum_{k \in C_i} r_{kj}\, \boldsymbol{\rho}_i^j \right] \tag{4}$$

where C_i is the set of indexes of the UAVs that send commands to i. We show next how this achieves scale consistency. Denote as $\mathbf{x_i^{d,j}}$ and $\mathbf{x_i}$ the ground positions associated with $\mathbf{p_i^{d,j}}$ and $\mathbf{p_i^j}$, respectively. Consider, without loss of generality, the robots' positions and image projections expressed in unknown equally oriented frames common to all cameras. As $\boldsymbol{\rho}_i^j = \mathbf{p_i^{d,j}} - \mathbf{p_i^j} = r_j(\mathbf{x_i^{d,j}} - \mathbf{x_i})$, (4) can be expressed as

$$\boldsymbol{\rho}_i^g = \overline{r}_i \sum_{j \in C_i} \left(\mathbf{x_i^{d,j}} - \mathbf{x_i}\right) \tag{5}$$

where the factor, which is unknown to all aerial units and robots

$$\overline{r}_i = \frac{1}{\text{card}(C_i)} \sum_{k \in C_i} r_k \tag{6}$$

is the average relative scale for the cameras that control robot i. Thus, the proposed scale adjustment in (4) makes the vectors $\boldsymbol{\rho}_i^j$ enter the computation of $\boldsymbol{\rho}_i^g$ with a consistent scale.

B. Control Law

Robot i computes (4) in its own frame, and

$$\rho_{\text{mi}} = \left\|\boldsymbol{\rho}_i^g\right\|, \quad \alpha_{\text{mi}} = \pi - \text{atan2}\left(\left(\boldsymbol{\rho}_i^g\right)_y, \left(\boldsymbol{\rho}_i^g\right)_x\right) \tag{7}$$

considering the robot's frame defined by its heading. The control goal for the robot is given by the ground position associated with the endpoint of its global motion vector. The variables α_i and ρ_i (see Fig. 3) express this position. As $\alpha_i = \alpha_{\text{mi}}$ and ρ_i is proportional to ρ_{mi}, we can control the robot using the image quantities. The proposed control law for robot i is

$$\begin{cases} v_i = -k_v\, \text{sign}(\cos\alpha_{\text{mi}})\, \rho_{\text{mi}} \\ \omega_i = k_\omega\, (\alpha_{\text{di}} - \alpha_{\text{mi}}) \end{cases} \tag{8}$$

where $k_v > 0$ and $k_\omega > 0$ are control gains, ω_i is considered in the counterclockwise direction, and we define

$$\alpha_{\text{di}} = \begin{cases} 0 & \text{if } |\alpha_{\text{mi}}| \le \dfrac{\pi}{2} \\ \pi & \text{if } |\alpha_{\text{mi}}| > \dfrac{\pi}{2} \end{cases}.$$

Angles are taken in $[-\pi, \pi)$. Observe that $0 \leq |\alpha_{\text{mi}} - \alpha_{\text{di}}| \leq \pi/2$ and that if $\cos\alpha_{\text{mi}} = 0$, $v_i = 0$ and robot i can rotate in place but not translate. We define α_{mi} as 0 if $\rho_{\text{mi}} = 0$.

Remark 1: From (5) and due to Property 1, a given robot's *direction* of motion is independent of the cameras' locations and calibrations. Therefore, clearly, these factors do not affect the stability of the controller, studied in Section V. The height and calibration of the cameras influence the value of $\overline{r}_i$, having an effect equivalent to an unknown positive multiplicative gain acting on the linear velocity control (8).

V. Stability Analysis

We study next the stability of the formation controller. We will consider common frames, only for analysis—recall that each UAV computes the control in its local image frame. Consider the robots' ground positions $\mathbf{x_i} = [x_i, y_i]^T$, $i = 1, \ldots, n$ expressed in an arbitrary global frame. We define the following cost function for the system under a topology $p \in \mathcal{P}$:

$$V = \sum_{j=1,\ldots,m} V^j, \quad V^j = \frac{1}{2} \sum_{i \in S_j^c} \left\| \mathbf{x_i^{d,j}} - \mathbf{x_i} \right\|^2. \tag{9}$$

Note that the state of the formation can be represented by the set of vectors $\mathbf{x_i^{d,j}} - \mathbf{x_i}$, $j = 1, \ldots, m$, $i \in S_j^c$, and V is radially unbounded, as $\left\| \mathbf{x_i^{d,j}} - \mathbf{x_i} \right\| \to \infty$ for a pair i and j implies $V \to \infty$. For generality, we use an alternative definition, common across all topologies, of the system's state, by defining the following stack state vector: $\mathbf{X} = [\mathbf{X_1}^T, \mathbf{X_2}^T, \ldots, \mathbf{X_n}^T]^T \in \mathbb{R}^{2n}$, where $\mathbf{X_i} = \mathbf{x_i^d} - \mathbf{x_i}$, and $\mathbf{x_i^d} = [x_i^d, y_i^d]^T$ is the ground position associated with the desired image point $\mathbf{p_i^d}$ obtained from any *global* similarity (i.e., one computed from all the n robots). Next, we establish two preliminary results.

Lemma 2: For any $p \in \mathcal{P}$, the robots form the desired shape if and only if $\mathbf{X} = \mathbf{0}$, which occurs if and only if $V = 0$.

Proof (Sketch): If $V^j = 0$ $\forall j$, we have all desired subshapes which, due to TC1, clearly fit together. When in the desired shape, desired and current points coincide, so $V = 0$. ■

Lemma 3: For any topology $p \in \mathcal{P}$, it holds $\forall j = 1, \ldots, m$, $\forall i \in S_j^c$ that $\partial V^j / \partial \mathbf{x_i} = \mathbf{x_i} - \mathbf{x_i^{d,j}}$.

Proof: Consider a camera j and, without loss of generality, that the frames for $j's$ current image points, and the associated ground positions, are equally oriented and centered on their centroids, $\mathbf{c_p^j}$ and $\mathbf{c_x^j}$. The values $\mathbf{p_{ic}^{\prime j}}$ are projections of equivalent template ground positions $\mathbf{x_{ic}^{\prime j}}$; so, for $i \in S_j^c$

$$\mathbf{p_{ic}^{\prime j}} = r_j \mathbf{x_{ic}^{\prime j}}, \quad \mathbf{p_i^j} = r_j \mathbf{x_i}, \quad \mathbf{p_i^{d,j}} = r_j \mathbf{x_i^{d,j}}. \tag{10}$$

As $\mathbf{p_i^{d,j}} = \mathbf{H_s^j}\, \mathbf{p_{ic}^{\prime j}}$, we have $\mathbf{x_i^{d,j}} = \mathbf{H_s^j}\, \mathbf{x_{ic}^{\prime j}}$, and we can write

$$V^j = \frac{1}{2} \sum_{i \in S_j^c} \left\| \mathbf{x_i^{d,j}} - \mathbf{x_i} \right\|^2 = \frac{1}{2} \sum_{i \in S_j^c} \left\| \mathbf{H_s^j} \mathbf{x_{ic}^{\prime j}} - \mathbf{x_i} \right\|^2. \tag{11}$$

Clearly, if $\mathbf{H_s^j}$ fits, with least-squares error, the template ($\mathbf{p_{ic}^{\prime j}}$) and current ($\mathbf{p_i^j}$) image points (Section III), it also does so for the positions ($\mathbf{x_{ic}^{\prime j}}$, $\mathbf{x_i}$). As V^j expresses precisely this sum of squared errors, $\mathbf{H_s^j}$ is the similarity that minimizes V^j. Considering that this transformation is unique and a differentiable function of the input points [29], $\partial V^j / \partial \mathbf{H_s^j}$ is null. It is then direct that $\partial V^j / \partial \mathbf{x_i} = \mathbf{x_i} - \mathbf{x_i^{d,j}}$ $\forall i \in S_c^j$, as claimed. ■

We now present the following main stability result.

Theorem 4: For any fixed topology $p \in \mathcal{P}$, by using the control law (8), the positions of the team of ground robots converge asymptotically to the desired formation shape.

Proof: We consider, without loss of generality, that all ground positions are expressed in a common frame, with which all image frames are aligned. We take V as a candidate Lyapunov function for the system. Its dynamics are

$$\dot{V} = \sum_{j=1}^{m} \left[\sum_{i \in S_j^c} \left(\frac{\partial V^j}{\partial \mathbf{x_i}} \right)^T \dot{\mathbf{x}}_\mathbf{i} \right]. \tag{12}$$

From (8), (5), and the unicycle kinematic model, we have

$$\dot{\mathbf{x}}_\mathbf{i} = k_v \mathbf{Q_i} \boldsymbol{\rho}_\boldsymbol{i}^\boldsymbol{g} = k_v \overline{r}_i \mathbf{Q_i} \sum_{j \in C_i} \left(\mathbf{x_i^{d,j}} - \mathbf{x_i} \right) \tag{13}$$

where the misalignment between the robot's displacement direction and $\boldsymbol{\rho}_\boldsymbol{i}^\boldsymbol{g}$ is captured by $\mathbf{Q_i} \in SO(2)$, a rotation by the angle $\alpha_{\text{mi}} - \alpha_{\text{di}}$. Substituting (13) and Lemma 3 in (12) gives

$$\begin{aligned} \dot{V} &= \sum_{j=1}^{m} \left\{ \sum_{i \in S_j^c} \left[\left(\mathbf{x_i} - \mathbf{x_i^{d,j}} \right)^T \left(k_v \overline{r}_i \mathbf{Q_i} \sum_{j \in C_i} \left(\mathbf{x_i^{d,j}} - \mathbf{x_i} \right) \right) \right] \right\} \\ &= -k_v \sum_{i=1}^{n} \overline{r}_i \cos(\alpha_{\text{mi}} - \alpha_{\text{di}}) \left\| \sum_{j \in C_i} \left(\mathbf{x_i^{d,j}} - \mathbf{x_i} \right) \right\|^2 \leq 0 \end{aligned} \tag{14}$$

where the inequality holds as $0 \leq |\alpha_{\text{mi}} - \alpha_{\text{di}}| \leq \pi/2$. From the invariant set theorem, the system is locally stable with respect to $V = 0$, i.e., the desired team shape (Lemma 2). We can guarantee global asymptotic stability, if the only equilibrium (i.e., $\dot{V} = 0$) of the system occurs at $\mathbf{X} = \mathbf{0}$ (i.e., $V = 0$). Due to the unicycle kinematics, $\dot{V}$ may be zero if no robot is translating, and at least one of them satisfies $\cos(\alpha_{\text{mi}} - \alpha_{\text{di}}) = 0$ and $\|\boldsymbol{\rho}_\mathbf{i}^\mathbf{g}\| > 0$. However, these robots will rotate in place at that moment, immediately making $\dot{V} < 0$. Hence, the only relevant scenario to examine is $\|\boldsymbol{\rho}_\mathbf{i}^\mathbf{g}\| = 0, i = 1, \ldots, n$. Using the topological conditions TC1–TC5 and the constraints they impose on the robots' motion vectors, and via a similar analysis to the one presented in the proof of [23, Corollary 1], one can see through simple geometric conditions that if a sum vector $\boldsymbol{\rho}_\mathbf{i}^\mathbf{g}$ is null, the individual vectors $\boldsymbol{\rho}_\mathbf{i}^\mathbf{j}$ must be null, too. Thus, the only possible stable equilibrium occurs at $V = 0$, i.e., the team of robots converges asymptotically to the prescribed shape. ■

Corollary 5: It is direct to see that the robots remain static once the desired shape has been achieved.

Corollary 6: The distance between every two robots remains upper-bounded with control law (8), for any topology $p \in \mathcal{P}$.

Proof: For finite initial robot positions, V (9) is clearly upper-bounded and, as $\dot{V} \leq 0$ (Theorem 4), it remains so for all time. As V is the sum of squared norms of the vectors

$\mathbf{x_i} - \mathbf{x_i^{d,j}}$, all these norms are also always upper-bounded, and so are the norms of $\rho_\mathbf{i}^\mathbf{j}$ (2) and, therefore, the norms of the motion vectors $\rho_\mathbf{i}^\mathbf{g}$ (4). Therefore, the magnitudes of the linear velocities for all robots (8) are also always upper-bounded, and the distance between any two robots may only become unbounded in infinite time. We can now consider, for all practical purposes, an arbitrarily small positive threshold b_{th} that stops the robots' motions (i.e., $\forall i$, $v_i = \omega_i = 0$ if $\rho_{\text{mi}} < b_{\text{th}}$). Then, since all robots will clearly—due to the vanishing behavior of V—stop displacing in finite time, the interrobot distances will be upper-bounded. ■

Corollary 7: For $p \in \mathcal{Q}$, clearly, Lemma 2 holds and, thanks to Theorem 4, the formation controller is locally stable.

Corollary 8: For the particular case $m = 1$, $S_1^c = S$ (i.e., a single UAV controls all the ground robots), it is direct from Theorem 4 that the formation controller is globally convergent.

Remark 9: The control may have singularities for certain robot arrangements that are nonattracting and have zero measure [23], [29]. Thus, for all practical purposes, $\mathbf{H_s^j}$ is differentiable (Lemma 3) and the system is stable. Alternatively, we could consider the degenerate cases and use an *almost-global* stability result. Also, even if control law (8) is discontinuous, the vanishing behavior of V suffices to prove stability. As the angular velocity in (8) always drives the system *away from* these discontinuities, chattering-like behaviors are not feasible.

A. Stability With Changes in Topology

Due to the motion of UAVs and ground robots during execution, the latter may come in and out of the fields of view of the cameras, so the sets S_j and S_j^c will switch. This affects $\mathbf{H_s^j}$ (1) and in turn, via $\mathbf{p_i^{d,j}}$ (Algorithm 1) and (2), (4), (7), it finally affects the control law (8). Thus, due to the topology changes, ours is a *switched system* [30], which we analyze as follows.

Proposition 10: Consider that the controller switches within the possible topologies $p \in \mathcal{P}$. Then, there exists a finite positive value τ_d such that the team of robots under control law (8) converges asymptotically to the formation shape if the average dwell time of every topology is at least τ_d.

Proof: $\mathcal{P}$ is a finite set, and the system's state (determined by the agents' positions) does not jump at switching times. Also, the dwell time of every topology is lower-bounded by a positive value (Section II). From Theorem 4, the formation is asymptotically stable for every individual p. All topologies drive the system to the same common equilibrium ($\mathbf{X} = \mathbf{0}$), but each has a different Lyapunov function—i.e., V_p for topology p. Thus, from [30], [31], there is a finite average dwell time that guarantees asymptotic stability if

$$V_p(\mathbf{X}) \leq \mu V_q(\mathbf{X}) \quad \forall \mathbf{X} \in \mathbb{R}^{2n} \quad \forall p, q \in \mathcal{P} \tag{15}$$

for a given constant μ. The Lyapunov function for a given topology consists of the sum of squared metric distances. Let us call these distances $d_i^j = \|\mathbf{x_i^{d,j}} - \mathbf{x_i}\|$. If $\mathbf{X} = \mathbf{0}$, all $d_i^j = 0$ for all topologies. Otherwise, there is at least one $d_i^j > 0$ for every topology. Denote as d_i^{j*} those d_i^j that are strictly positive. From Corollary 6, for all the topologies, interrobot distances remain upper-bounded; therefore, the desired positions $\mathbf{x_i^{d,j}}$ are such that all d_i^{j*} are always upper-bounded, too. Therefore, the ratio of any two d_i^{j*} is bounded—i.e., we can define a finite value $B = \max_{i,j,p,\mathbf{X}}(d_i^{j*}) / \min_{i,j,p,\mathbf{X}}(d_i^{j*})$. Now, as each Lyapunov function is the sum of a finite number of d_i^j distances squared, it follows that a finite μ in (15) must exist. Hence, the statement of the proposition holds true. ■

This result means that if every topology is active, on average, for a sufficiently long time, the desired ground team shape will be attained. Other interesting properties are that the switching is controllable—the aerial units can, through their coordinated motions and decisions, determine the switches—and typically will stop in finite time—clearly, when the ground team is close to the prescribed shape, no topology switches are needed.

VI. Motion and Coordination of the Aerial Units

We give next guidelines to implement the aspects of UAV control and coordination, whose detailed study is not the focus of this brief. A key observation is that high-speed and precise aerial unit motions are not required: the UAVs do not need to react fast or reach specific positions, the control is inherently robust to imperfect UAV motions (Remark 1), and we can define safety margins to aid their maneuverability. Thus, it is reasonable to model the UAV translational motion at a kinematic—and not dynamic—control level [28]. For simplicity, in our tests, we use single-integrator kinematics.

In terms of their coordination, we propose to make the UAVs follow the algorithm in [23], which exploits communications (Section II) of image data and ensures TC1 and TC2 by preserving the links of the initial graph $\mathcal{G}_c(t = 0)$. To initially deploy the UAVs without full knowledge of the ground robot locations, distributed coverage/search algorithms with connectivity maintenance features can be used. A simple approach can be, e.g., to deploy the UAVs one-by-one sequentially while enforcing TC1 and TC2 and create an initial path graph $\mathcal{G}_c$. Note that each UAV controls its displacement to preserve in the field of view the *two* closest robots seen in common with each one of its neighbors in $\mathcal{G}_c$; thus, additional common robots can leave the UAV's control scope as the system evolves (i.e., transfers of robots between UAVs are possible). TC1–TC5 can be met by suitably defining S_j^c (which are subsets of S_j, $\forall j$) via distributed protocols, implemented for a duo of neighboring UAVs using, e.g., image distance-based criteria. The duo can thus decide which two of their common viewed ground robots they will share the control over, and which of the two UAVs will assume (if needed) control of the other common viewed robots. The activation time of each topology can also be ensured to be lower bounded. The exchanged data (S_j and image points) between neighboring UAVs could be used in more efficient and flexible coordination schemes to, e.g., balance the load (i.e., cardinality of sets S_j^c), and recover the affected ground robots if a UAV fails.

VII. Simulation Results

In this section, we illustrate the performance of the control method with simulations. We first describe an example

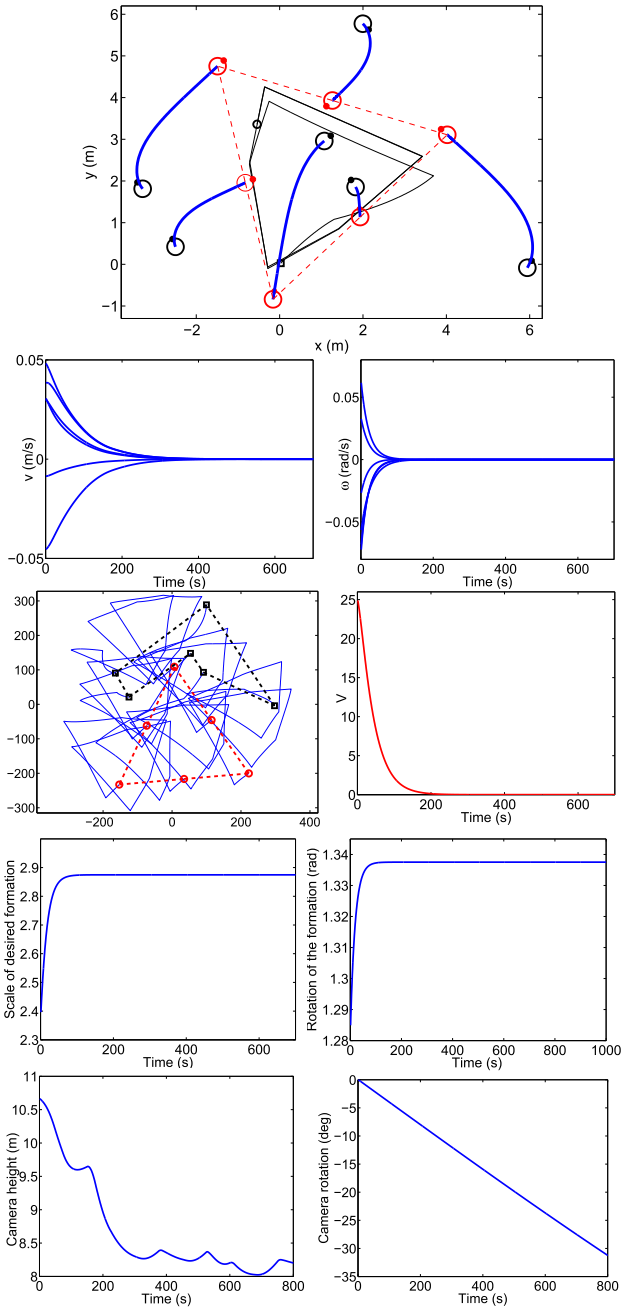

Fig. 4. One-camera simulation results. Row 1: robot paths (final positions joined by dashed lines) and projection of camera path on ground plane (initial point marked as square and final point marked as circle). Row 2: linear (left) and angular (right) robot velocities. Row 3: image traces of robots (left)—initial and final point sets joined by dashed lines—and cost function (right). Row 4: scale (left) and rotation (right) of desired formation. Row 5: camera height (left) and rotation (right).

where one downward-facing camera was used to drive a group of six unicycle robots to a triangular desired shape. Fig. 4 displays the results, showing how the formation was achieved. The aerial unit was displaced horizontally following the perimeter of the ground formation. By doing so—instead of, e.g., remaining over the team's centroid—it can gain a richer perception of the ground team's surroundings so as to, e.g., detect obstacles or threats. Note that this persistent UAV motion does not affect the formation's convergence. The camera always maintained a good visibility of all the robots, as seen in the image traces. The UAV controlled its vertical motion to guarantee this visual coverage, and it also rotated during execution. We stress that the UAV used only image information, expressed in pixels.

In another example, three aerial units controlled a team of 16 robots, to make them form a star-shaped configuration. Throughout the simulation, the UAVs moved as discussed in Section VI and generated ground control commands as described in Section IV. Each unit j controlled those robots in S_j closer than certain safety thresholds to the center of the image. The three cameras had different calibrations. The UAVs only translated and did not rotate. Each had a different orientation. The results in Fig. 5 illustrate how the desired ground shape was achieved. There were topology switches, which caused the discontinuous changes observable in the plots. The cameras eventually stabilized to fixed positions. The plots show the scales and rotations of the *partial* formations controlled by the UAVs, expressed in an arbitrary common fixed reference unknown to any UAV (note that these are *not* the scales and rotations of the image similarities [see (1)], which remain different for each camera and change continuously as they move). As expected, the three scales and rotations end up being equal as the team acquires the prescribed shape.

VIII. Practical Discussion and Conclusion

We first discuss some application details and advantages and then limitations and potential improvements of our method.

1) The proposed multi-UAV hybrid topology is scalable—it can include an arbitrarily large number of ground robots, and workspace—and reliable—there is no central point of failure.
2) The ground robots are freed from sensing, costly processing, and wireless transmission. Thus, one can use simple, low-cost robots which will also have higher autonomy due to reduced power consumption. Their resources can hence be focused on other tasks (e.g., environmental monitoring or exploration).
3) The UAVs do not have to achieve a specific relative positioning or to synchronize their orientations. Thus, they are free to consider other concurrent goals—aside from ground formation achievement—and, hence, fully exploit the known advantages of heterogeneous air/ground teams [19], [25]: they can monitor and preserve the system connectivity, reconfigure in case of failures, and their rich aerial imaging can enhance the navigation capabilities of the ground robots.
4) As it does not need camera calibration and knowledge of scene scale, our method is robust to calibration errors and drifts—which are known to affect visual control stability—allows to mount or change the cameras without preparative procedures, and, e.g., directly allows the use of zoom—which is clearly a very powerful feature for the scenario and the task we consider.
5) Clearly, the UAVs will need to have localization information to enable them to navigate, which can be

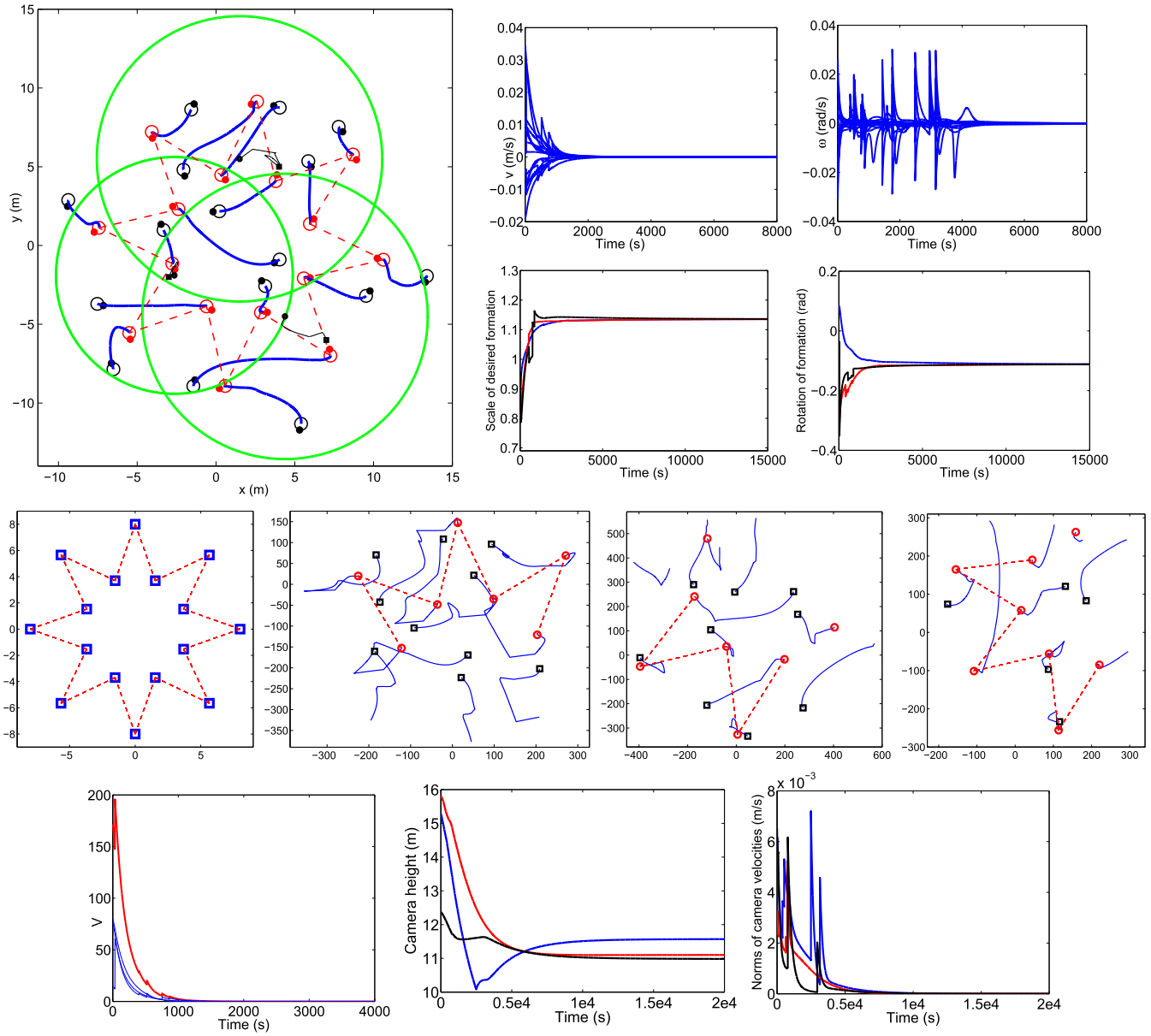

Fig. 5. Simulation results. Top left: robot paths (final positions joined by dashed lines), final camera fields of view (circles), and paths of the three cameras. Top-right: evolution of linear and angular velocities of the ground robots (top) and scales and rotations of the partial desired formations (bottom). Second row: template image (left), and image traces of the robots in S_j^c for the three cameras (initial points marked as squares, final points marked as circles, and joined by dashed lines). Bottom row: evolution of V (highest valued curve) and the three V^j (left), camera heights (center), and camera velocity norms (right).

available in the infrastructure-free scenario we consider via, e.g., existing visual-inertial approaches. Our ground control is robust to errors in this information as it does not employ it.

6) By using only *local* (image) measurements, our method avoids the issues associated with using a shared UAV reference frame: need to maintain the agreed frame (requiring consensus or synchronization), inaccuracies in its definition—and their propagation among UAVs—or inter-UAV communication issues (temporary losses and multihop delays. . .).

In summary, our method demands only simple resources from the ground robots and does not need a complex coordination strategy for the UAVs, provides a flexible architecture, and has useful decoupling properties and robustness to various typical sources of error. All these properties facilitate simpler implementation and integration of other tasks (aerial and ground perception/actuation) with the formation control itself.

Limitations and Possible Improvements: Although the two-layer architecture provides distribution, the failure of a UAV affects not one but multiple robots—until other UAVs recover from it. Also, it can be hard to visually detect and identify all robots in challenging conditions. Using interchangeable robots could be more robust and efficient, at the cost of more complex coordination. Performance will be perturbed if UAV disturbances make the camera not face downward—although image rectification as in [21] can mitigate this—or there are terrain irregularities. Finally, collision

avoidance—e.g., via reactive methods—for robots and UAVs should be used.

REFERENCES

[1] M. Mesbahi and M. Egerstedt, *Graph Theoretic Methods in Multiagent Networks*. Princeton, NJ, USA: Princeton Univ. Press, 2010.

[2] B. D. O. Anderson, C. Yu, and J. M. Hendrickx, "Rigid graph control architectures for autonomous formations," *IEEE Control Syst. Mag.*, vol. 28, no. 6, pp. 48–63, Dec. 2008.

[3] J. Cortés, "Global and robust formation-shape stabilization of relative sensing networks," *Automatica*, vol. 45, no. 12, pp. 2754–2762, 2009.

[4] W. Ren, "Consensus tracking under directed interaction topologies: Algorithms and experiments," *IEEE Trans. Control Syst. Technol.*, vol. 18, no. 1, pp. 230–237, Jan. 2010.

[5] X. Cai and M. de Queiroz, "Adaptive rigidity-based formation control for multirobotic vehicles with dynamics," *IEEE Trans. Control Syst. Technol.*, vol. 23, no. 1, pp. 389–396, Jan. 2015.

[6] K. K. Oh, M. C. Park, and H. S. Ahn, "A survey of multi-agent formation control," *Automatica*, vol. 53, pp. 424–440, Mar. 2015.

[7] A. N. Bishop, I. Shames, and B. D. O. Anderson, "Stabilization of rigid formations with direction-only constraints," in *Proc. IEEE Conf. Decision Control Eur. Control Conf.*, Dec. 2011, pp. 746–752.

[8] T. Eren, "Formation shape control based on bearing rigidity," *Int. J. Control*, vol. 85, no. 9, pp. 1361–1379, 2012.

[9] A. Franchi and P. R. Giordano, "Decentralized control of parallel rigid formations with direction constraints and bearing measurements," in *Proc. IEEE Conf. Decision Control*, Dec. 2012, pp. 5310–5317.

[10] S. Coogan and M. Arcak, "Scaling the size of a formation using relative position feedback," *Automatica*, vol. 48, no. 10, pp. 2677–2685, 2012.

[11] E. Schoof, A. Chapman, and M. Mesbahi, "Bearing-compass formation control: A human-swarm interaction perspective," in *Proc. Amer. Control Conf.*, 2014, pp. 3881–3886.

[12] Z. Lin, L. Wang, Z. Han, and M. Fu, "Distributed formation control of multi-agent systems using complex Laplacian," *IEEE Trans. Autom. Control*, vol. 59, no. 7, pp. 1765–1777, Jul. 2014.

[13] S. Zhao and D. Zelazo, "Bearing rigidity and almost global bearing-only formation stabilization," *IEEE Trans. Autom. Control*, vol. 61, no. 5, pp. 1255–1268, May 2016.

[14] D. Zelazo, P. R. Giordano, and A. Franchi, "Bearing-only formation control using an SE(2) rigidity theory," in *Proc. IEEE Conf. Decision Control*, Dec. 2015, pp. 6121–6126.

[15] Z. Han, L. Wang, Z. Lin, and R. Zheng, "Formation control with size scaling via a complex Laplacian-based approach," *IEEE Trans. Cybern.*, vol. 46, no. 10, pp. 2348–2359, Oct. 2016.

[16] N. Moshtagh, N. Michael, A. Jadbabaie, and K. Daniilidis, "Vision-based, distributed control laws for motion coordination of nonholonomic robots," *IEEE Trans. Robot.*, vol. 25, no. 4, pp. 851–860, Aug. 2009.

[17] E. Montijano, J. Thunberg, X. Hu, and C. Sagüés, "Epipolar visual servoing for multirobot distributed consensus," *IEEE Trans. Robot.*, vol. 29, no. 5, pp. 1212–1225, Oct. 2013.

[18] N. Michael, J. Fink, and V. Kumar, "Controlling ensembles of robots via a supervisory aerial robot," *Adv. Robot.*, vol. 22, no. 12, pp. 1361–1377, 2008.

[19] S. Lacroix and G. Le Besnerais, "Issues in cooperative air/ground robotic systems," in *Robotics Research*. Berlin, Germany: Springer, 2011, pp. 421–432.

[20] M. Schwager, B. J. Julian, M. Angermann, and D. Rus, "Eyes in the sky: Decentralized control for the deployment of robotic camera networks," *Proc. IEEE*, vol. 99, no. 9, pp. 1541–1561, Sep. 2011.

[21] G. López-Nicolás, M. Aranda, Y. Mezouar, and C. Sagüés, "Visual control for multirobot organized rendezvous," *IEEE Trans. Syst., Man, Cybern. B, Cybern.*, vol. 42, no. 4, pp. 1155–1168, Aug. 2012.

[22] L. R. G. Carrillo, G. R. F. Colunga, G. Sanahuja, and R. Lozano, "Quad rotorcraft switching control: An application for the task of path following," *IEEE Trans. Control Syst. Technol.*, vol. 22, no. 4, pp. 1255–1267, Jul. 2014.

[23] M. Aranda, G. López-Nicolás, C. Sagüés, and Y. Mezouar, "Formation control of mobile robots using multiple aerial cameras," *IEEE Trans. Robot.*, vol. 31, no. 4, pp. 1064–1071, Aug. 2015.

[24] F. Poiesi and A. Cavallaro, "Distributed vision-based flying cameras to film a moving target," in *Proc. IEEE/RSJ Int. Conf. Intell. Robots Syst.*, Sep./Oct. 2015, pp. 2453–2459.

[25] J. Chen, X. Zhang, B. Xin, and H. Fang, "Coordination between unmanned aerial and ground vehicles: A taxonomy and optimization perspective," *IEEE Trans. Cybern.*, vol. 46, no. 4, pp. 959–972, Apr. 2016.

[26] R. Olfati-Saber, J. A. Fax, and R. M. Murray, "Consensus and cooperation in networked multi-agent systems," *Proc. IEEE*, vol. 95, no. 1, pp. 215–233, Jan. 2007.

[27] K. Liu, Z. Ji, G. Xie, and L. Wang, "Consensus for heterogeneous multi-agent systems under fixed and switching topologies," *J. Franklin Inst.*, vol. 352, no. 9, pp. 3670–3683, Sep. 2015.

[28] O. Bourquardez, R. Mahony, N. Guenard, F. Chaumette, T. Hamel, and L. Eck, "Image-based visual servo control of the translation kinematics of a quadrotor aerial vehicle," *IEEE Trans. Robot.*, vol. 25, no. 3, pp. 743–749, Jun. 2009.

[29] J. C. Gower and G. B. Dijksterhuis, *Procrustes Problems*. London, U.K: Oxford Univ. Press, 2004.

[30] D. Liberzon, *Switching in Systems and Control*. Boston, MA, USA: Birkhäuser, 2003.

[31] J. P. Hespanha and A. S. Morse, "Stability of switched systems with average dwell-time," in *Proc. IEEE Conf. Decision Control*, Dec. 1999, pp. 2655–2660.